



OPEN

Natural variability in air–sea gas transfer efficiency of CO₂

Mingxi Yang^{1✉}, Timothy J. Smyth¹, Vassilis Kitidis¹, Ian J. Brown¹, Charel Wohl¹, Margaret J. Yelland² & Thomas G. Bell¹

The flux of CO₂ between the atmosphere and the ocean is often estimated as the air–sea gas concentration difference multiplied by the gas transfer velocity (K_{660}). The first order driver for K_{660} over the ocean is wind through its influence on near surface hydrodynamics. However, field observations have shown substantial variability in the wind speed dependencies of K_{660} . In this study we measured K_{660} with the eddy covariance technique during a ~11,000 km long Southern Ocean transect. In parallel, we made a novel measurement of the gas transfer efficiency (GTE) based on partial equilibration of CO₂ using a Segmented Flow Coil Equilibrator system. GTE varied by 20% during the transect, was distinct in different water masses, and related to K_{660} . At a moderate wind speed of 7 m s⁻¹, K_{660} associated with high GTE exceeded K_{660} with low GTE by 30% in the mean. The sensitivity of K_{660} towards GTE was stronger at lower wind speeds and weaker at higher wind speeds. Naturally-occurring organics in seawater, some of which are surface active, may be the cause of the variability in GTE and in K_{660} . Neglecting these variations could result in biases in the computed air–sea CO₂ fluxes.

The ocean has absorbed roughly a quarter to a third of anthropogenic CO₂ emissions since the industrial revolution^{1,2}. About half of the global oceanic CO₂ uptake occurs in the Southern Ocean^{3,4}—a vast, poorly observed region with areas of deepwater formation that sequesters carbon from the surface⁵. Air–sea CO₂ flux is generally estimated as the product of the air–sea CO₂ concentration difference and the CO₂ gas transfer velocity (here denoted as K_{660}). There remains substantial (at least 25%) uncertainty in the estimation of air–sea CO₂ flux⁶, in large part due to uncertainty and variability in K_{660} ⁷. This limits our ability to accurately assess the current carbon cycle and predict future climate scenarios.

Wind provides the primary turbulent forcing for air–sea exchange by governing near surface hydrodynamics⁸. As a result, K_{660} is typically parameterized solely as a function of wind speed. However, mean wind speed dependencies in K_{660} derived from recent air–sea CO₂ flux measurements in the Southern Ocean^{9–11} vary considerably (~20% at intermediate wind speeds and ~100% at low and high wind speeds; see supplement). Waves^{12,13}, bubbles^{9,14,15}, and surfactants^{16–18} (focus of this study) have been proposed as additional controlling factors for K_{660} .

A myriad of different natural organic materials exists in the surface ocean, varying in concentration, molecular size, solubility, and surface activity. The more surface active organics, or surfactants, tend to be more concentrated near the air–sea interface (within a ca. 100 μm depth region often called the sea surface microlayer, or SML) relative to the waters below. Surfactants can be roughly divided into insoluble and soluble types, which are thought to affect gas transfer through different mechanisms. Insoluble surfactants can form film or slicks, providing additional barrier to air–sea transfer (e.g. ref.¹⁹). Such insoluble surfactant films are quickly dispersed by wind and waves and are thus likely to be important only during very calm conditions²⁰. Soluble surfactants impact gas transfer across a wider range of wind conditions by changing the surface ocean hydrodynamics²¹. Recent surveys of surfactants in SML (a challenging measurement in situ) demonstrate that they are ubiquitously present in the global oceans with large variability in concentration (~60 μg L⁻¹ to a few mg L⁻¹ Triton-X-100 equivalent^{18,22}).

Tank experiments show that naturally occurring surfactants can suppress the rate of gas transfer by 10–50% (e.g. oxygen by ref.^{23,24}; methane by ref.^{17,25}). A direct relationship was reported between gas transfer suppression in a tank and the surfactant concentration in SML waters^{17,25}. Organic materials excreted from marine phytoplankton, including carbohydrates associated with proteins and possibly lipids, appear to be the principal classes of molecules responsible for gas transfer suppression¹⁶. The main drawback of these studies is that the nature of turbulence in the upper ocean cannot easily be compared with the turbulence in the tanks (e.g. induced by a baffle in ref.²⁵, and by a shaker table in ref.^{16,23}).

¹Plymouth Marine Laboratory, Prospect Place, Plymouth, UK. ²National Oceanography Centre, European Way, Southampton, UK. ✉email: miya@pml.ac.uk

Field evidence of gas transfer suppression by natural surfactants is very limited. Frew et al.²⁴ inferred K_{660} from a thermal imaging technique in coastal waters at low wind speeds. They found that in the presence of natural surfactant films (identified by surface enrichment in the absorption of coloured dissolved organic matter, CDOM), the inferred gas transfer velocity was lower by up to an order of magnitude relative to the no-film case. Mustafa et al.¹⁸ coupled measurements of surfactant concentration with estimates of CO_2 transfer using a floating chamber at wind speeds less than 7 m s^{-1} in different parts of the Atlantic and Pacific oceans as well as in nearshore waters. Their measurements suggest a relative gas transfer suppression of 23% (sufficient surfactant present in SML, but no film) to 62% (surfactant film). It is unclear from these observations what the effect of surfactants might be on near surface hydrodynamics and hence on K_{660} at moderate to high wind speeds.

Here we directly measured the air–sea CO_2 flux using the eddy covariance method and the seawater fugacity of CO_2 during a recent shipboard transect in the Southern Ocean. This enabled us to derive K_{660} at wind speeds up to 18 m s^{-1} . In parallel, we present a novel measurement of the gas transfer efficiency (GTE) based on partial equilibration of CO_2 using a purpose-built, dual Segmented Flow Coil Equilibrator (SFCE) system. This system provides a quantification of the effect of varying seawater composition on gas transfer that is not directly driven by wind. We combine these observations to better understand the hydrodynamical processes that drive air–sea CO_2 transfer.

Methods

Eddy covariance measurements of air–sea CO_2 flux. Eddy covariance (EC) is the most direct method for observing the air–sea CO_2 flux and its application to shipboard measurements has been improved significantly in recent years^{26–28}. Briefly, the CO_2 flux is determined by correlating high frequency (here 10 Hz) fluctuations in the dry mixing ratio of atmospheric CO_2 ($x\text{CO}_2$) with those in the vertical wind velocity (w) and averaging over time (here 20 min): $x\text{CO}_2 w'$. Measurements of winds on a ship are affected by the ship's motion and by flow distortion due to the ship's superstructure²⁹. A sonic anemometer (Metek uSonic-3 Scientific) measuring 3D wind velocities as well as a motion sensor measuring 3D linear accelerations and rotational rates (Systron Donner Motionpak II) were installed on the foremast of the RRS James Clark Ross (JCR), 21.5 m above water. The motion data were used to correct the wind measurements for the ship motion following established methods^{12,26,30}, while three dimensional computational fluid dynamic modeling results for the JCR³¹ were used to correct the measured mean wind speed for flow distortion. The COARE 3.5 model³² was used to convert the observed true wind speed to 10-m neutral wind speed (U_{10n}). The 10-m neutral drag coefficient derived from eddy covariance (u_*^2/U_{10n}^2) closely agrees with the COARE 3.5 model, suggesting that both the motion and the flow distortion corrections are reasonable (Supplementary Fig. S1).

The CO_2 air intake was mounted 73 cm below the center volume of the Metek sonic anemometer, and the sample air was pulled rapidly through a 30 m length of 9.5 mm inner diameter (ID) Teflon tube by a dry vacuum pump (Gast 1023 series) at a flow rate of $\sim 40 \text{ L a minute}$ (LPM). A Picarro Cavity Ringdown Spectrometer (G2311-f) sub-sampled from the main inlet tube for the dry CO_2 mixing ratio at $\sim 5 \text{ LPM}$. Before entering the Picarro, sample air passed through a short section of 3.2 mm ID Teflon tube, a particle filter ($2 \mu\text{m}$), and a counter-flow dryer (Nafion PD-200T-24M). The dryer minimized the interference in CO_2 measurement due to water vapour (H_2O) by removing $\sim 80\%$ of the H_2O in the mean and almost all of the variability³³. The H_2O signal was measured concurrently by the Picarro instrument and was used to numerically remove the residual H_2O signal within the Picarro software³⁴, yielding the atmospheric CO_2 dry mixing ratio ($x\text{CO}_2$, in ppm) needed for the flux calculation.

Measuring CO_2 downstream of a long inlet tube and a dryer resulted in a delay in the CO_2 signal relative to the wind measurement and a small amount (ca. 10%) of high frequency attenuation in the flux signal. A puff of nitrogen gas was injected into the inlet tip once every 6 h. The decay in the gas signal (due to dilution by the nitrogen) was used to estimate both the delay time ($3.4 \pm 0.2 \text{ s}$) and the response time (0.36 s). The delay in the CO_2 signal is accounted for in the flux calculation, while the high frequency flux attenuation is corrected with a filter function approach using the measured response time (Landwehr et al. 2018). The Picarro instrument is sensitive to motion acceleration, yielding substantially higher variance in $x\text{CO}_2$ when the ship is in rough seas. The heave of the ship also means that the sample inlet moves vertically along a gradient in $x\text{CO}_2$ ²⁶. These motion effects are corrected for by decorrelating $x\text{CO}_2$ measurements with the ship's acceleration, velocity, and displacement¹². The flux in mixing ratio units (e.g. ppm m s^{-1}) is converted to molar fluxes (e.g. mmole $\text{m}^{-2} \text{ day}^{-1}$) using the dry density of air computed from air temperature, pressure, and humidity measurements.

The wind sector of ± 130 degrees (0 degree for directly over the bow) is considered for fluxes, excluding periods of contamination from ship's exhaust when the winds were from the aft. Additional quality control criteria for CO_2 flux are similar to ref.¹², and further include stationarity measures of wind^{35,36}. To reduce random noise, quality controlled 20-min fluxes are averaged to hourly intervals or averaged in wind speed bins (width of 2 m s^{-1}). The uncertainty in EC CO_2 flux is estimated empirically and propagated to K_{660} ($\sim 20\%$ for an hourly average). See Dong et al.³⁷ for further details on flux processing and uncertainty analysis.

Seawater $f\text{CO}_2$ and calculation of CO_2 gas transfer velocity (K_{660}). Measurements of high-resolution underway $f\text{CO}_2$ and gas transfer efficiency were made using two Segmented Flow Coil Equilibrator (SFCE) system deployed in parallel on the ANDREX II cruise. $f\text{CO}_2$ was additionally measured with a standard vented-showerhead equilibrator system coupled to an infrared gas analyzer³⁸. The SFCE, modified from earlier designs^{12,39}, has been described in detail by Wohl et al.⁴⁰. Briefly, ship's underway seawater (from $\sim 6 \text{ m}$ depth) was piped into a $\sim 200 \text{ mL}$ glass bottle via a $\sim 1 \text{ m}$ long 6.4 mm ID Teflon tube and allowed to overflow into the sink. For each SFCE, water was extracted from the bottom of this glass bottle by a peristaltic pump via a $\sim 0.5 \text{ m}$ long 4.0 mm ID Teflon tube and a $\sim 15 \text{ cm}$ long 4.4 mm ID Pumpsil soft, platinum-cured silicon tube. CO_2 -free

synthetic air was added continuously to the sample seawater at a Teflon ‘tee’ piece, naturally forming distinct, cm-long water and air segments. The air and water segments traveled in the same direction through a 4.0 mm ID Teflon tube, where gas transfer occurs. Water and air segments were then separated at an air–water separating ‘tee’. Sample air left from the top of the separator and flowed towards the CO₂ analyzer (Licor7000), while the sampled water was drained away from the bottom of the separator. The two SFCEs operated simultaneously and alternate CO₂ measurements were made with the same Licor7000 every five minutes (switching controlled by a solenoid valve). The water flow rate was controlled for each SFCE at 100 mL min⁻¹ by the peristaltic pump (flow monitored several times a day). The total synthetic airflow rate was set at 50 mL min⁻¹ by a mass flow controller, which was split evenly between the two SFCEs. Sample air was dried with a Nafion dryer and filtered with a Swagelok particle filter to reduce the influence of humidity and particulates on the CO₂ measurement. Compared to membrane-based equilibrators, advantages of the SFCE include rapid gas transfer (due to surface renewal within individual segments³⁹) and the absence of membranes that could become clogged due to bio-fouling. As a precautionary measure, the SFCEs were washed with 10% hydrochloric acid every few days to prevent any internal biological growth.

The two SFCE systems were identical except for the length of the gas transfer coil (20 m vs. 40 cm). The long coil was kept close to ambient sea surface temperature by immersion in a rapidly overflowing bucket of underway seawater. Continuous monitoring indicated that the bucket water temperature was consistently 1 °C higher than ambient water temperature, and this temperature difference was accounted for in the fCO₂ calculation below for thermally induced change in carbonate chemistry⁴¹. Measurement from the long coil (CO_{2, long}) is related to the dry CO₂ mixing ratio at equilibrium with ambient seawater (xCO_{2,w}) by a purge factor (PF): xCO_{2,w} = CO_{2, long} PF. Purging occurs because gas exchange with CO₂-free air reduces CO₂ in the aqueous phase, such that CO_{2, long} is lower than xCO_{2,w}. We define PF as the aqueous concentration before equilibration divided by the aqueous concentration after equilibration. At the low temperatures encountered during this transect (0.7 ± 0.5 °C), PF for underway seawater is well predicted by mass conservation⁴⁰:

$$PF = 1 + 1/(H Q_w/Q_a). \quad (1)$$

Here Q_w and Q_a indicate the flow rates of water and air, respectively, and H is the dimensionless solubility of CO₂ (water to air). For 0.7 °C seawater (cruise mean), PF was 1.176 for CO₂ at a water flow rate of 100 mL min⁻¹ and airflow rate of 25 mL min⁻¹.

Following ref.⁴¹, xCO_{2,w} derived from the long coil is converted to seawater fCO₂. Seawater fCO₂ derived from the long coil SFCE and from the widely used showerhead equilibrator demonstrate exceptionally good agreement during the ANDREXII cruise (Supplementary Fig. S2). This suggests near full equilibration of CO₂ within the long coil as well as high stability of the SFCE system. For the calculation of K_{660} , we use seawater fCO₂ from the showerhead equilibrator where available and use fCO₂ from the SFCE to fill any remaining gaps (see Fig. S2). Atmospheric fCO₂ (mean ± standard deviation of 390.6 ± 6.6 µatm) was subtracted from seawater fCO₂ to yield ΔfCO₂. Maps of the transect colour-coded by CO₂ flux and ΔfCO₂ are shown in Supplementary Fig. S3.

The CO₂ transfer velocity was computed as follows to facilitate comparison with previous measurements: $K_{CO_2} = \text{flux}/S/\Delta fCO_2$. Here S is the dimensional CO₂ solubility as a function of temperature and salinity⁴². K_{CO_2} is scaled to a Schmidt number of 660 assuming an exponent of -0.5: $K_{660} = K_{CO_2} (660/Sc)^{-1/2}$, where Sc is the ambient Schmidt number of CO₂⁴². To reduce random noise as well as any bias in K_{660} generated by dividing by very small ΔfCO₂, only K_{660} data with |ΔfCO₂| > 30 µatm are retained.

Derivation of the CO₂ gas transfer efficiency (GTE). The short coil SFCE system had a 40 cm long equilibrator tube. This length was purposely chosen such that CO₂ did not come to full equilibration in the short coil. GTE is calculated simply as the ratio between the measured CO₂ from the short coil (what has been transferred) and xCO_{2,w} (the initial potential for transfer). Triplicate measurements of the same water demonstrate that the precision in the GTE measurement is within 0.01. Our measurement setup was kept unchanged (including the geometry of the SFCEs and air/water flow rates) and the ambient seawater temperature was nearly constant (0.7 ± 0.5 °C) during this transect. Any variations in GTE were thus most likely driven by natural variability in seawater composition. Conceptually our measurement shares some similarities to those by ref.^{17,25}. Unlike those earlier observations, we do not reference GTE against pure water here, which avoids the difficulties associated with generating surfactant-free water.

Our underway measurement of GTE uses subsurface seawater (~6 m depth) rather than SML water. SML water would arguably be more directly relevant to air–sea transfer, although subsurface and SML water compositions have been shown to be closely coupled for most organic materials^{43,44} and for surfactant concentration^{18,22}. The continuous sampling of subsurface water is much easier logistically and enables a substantially larger dataset to be generated while avoiding the many possible artifacts from SML sampling^{45,46}. Discrete samples of deep seawater (typically below 1000 m) from the CTD rosette, generally thought to be devoid of labile organic compounds, were measured opportunistically (N = 8) for GTE. At approximately the same temperatures as the surface waters, these additional deepwater samples provide a reference for comparison for the underway GTE observations.

Results

Variability in gas transfer efficiency (GTE) and CO₂ gas transfer velocity (K_{660}). Figure 1 shows the track of the ANDREXII cruise (Feb–Apr 2019), colour-coded by the underway GTE. The mean (standard deviation) GTE was 0.573 (0.024), with a range of 0.507 to 0.623 (~20%). GTE displayed considerable variability on short temporal and small spatial scales that often coincided with water mass changes (see supplement). The frequency distribution of GTE was bimodal—the more frequent mode was associated with higher GTE, while

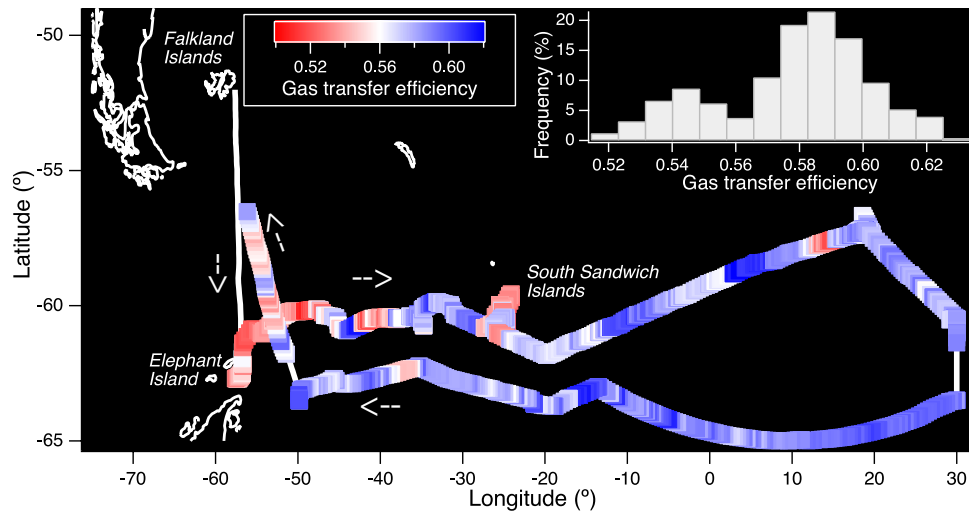


Figure 1. Cruise track colour-coded by the underway gas transfer efficiency, with the thick white line indicating no GTE measurement. The transect started and finished at the Falkland Islands. The return (westward) leg is displaced 2 degrees latitude south of the actual transect for clarity. GTE demonstrated substantial variability (see Supplement for further details) and a bimodal frequency distribution (inset).

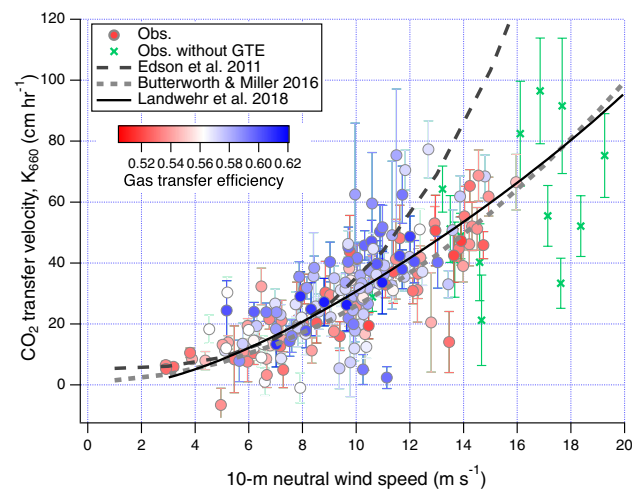


Figure 2. Air–sea CO_2 transfer velocity (hourly; $n = 199$) vs. 10-m neutral wind speed, scaled to a Schmidt number of 660 with an exponent of -0.5 and colour-coded by GTE. K_{660} observations without concurrent GTE measurements are denoted with crosses. K_{660} tends to be reduced when GTE was low, and vice versa. Also shown are the wind speed dependences from three direct measurements of CO_2 K_{660} , from ref.^{9–11}. The error bars on K_{660} are propagated from the empirically estimated EC flux uncertainty (see ref.³⁷).

the less frequent mode was associated with lower GTE. Low GTE values were observed on multiple occasions and were not limited to a single region (Fig. 1).

Observations of the CO_2 gas transfer velocity (K_{660}) are shown in Fig. 2 as a function of wind speed, along with mean relationships identified during three recent CO_2 air–sea gas transfer studies in the Southern Ocean. At moderate to high wind speeds, our observations span all of the previous wind speed relationships, but are in closer agreement in the mean (within $\sim 20\%$) with ref.^{9–11}. Wind speed explains 58% of the variance in K_{660} from this transect ($K_{660_fit} = -0.35 + 1.10U_{10m}^{1.46}$; see Supplementary Fig. S4). We note that even for observations with very high signal:noise ratios (e.g. ref.^{11,47}), the R^2 value between K_{660} and wind speed is at most around 0.8, implying that at least 20% of the variance in K_{660} may be due to factors other than wind speed. While averaging in wind speed bins helps to reduce the random uncertainty in K_{660} , doing so likely masks the variability in gas transfer caused by these other processes, which we explore next.

Relationship between K_{660} and GTE. K_{660} in Fig. 2 is colour-coded by GTE to illustrate the effect of varying hydrodynamics. It appears that at a given wind speed, K_{660} values associated with high GTE tend to cluster above K_{660} values associated with low GTE—an effect most obvious at moderate wind speeds. To examine this

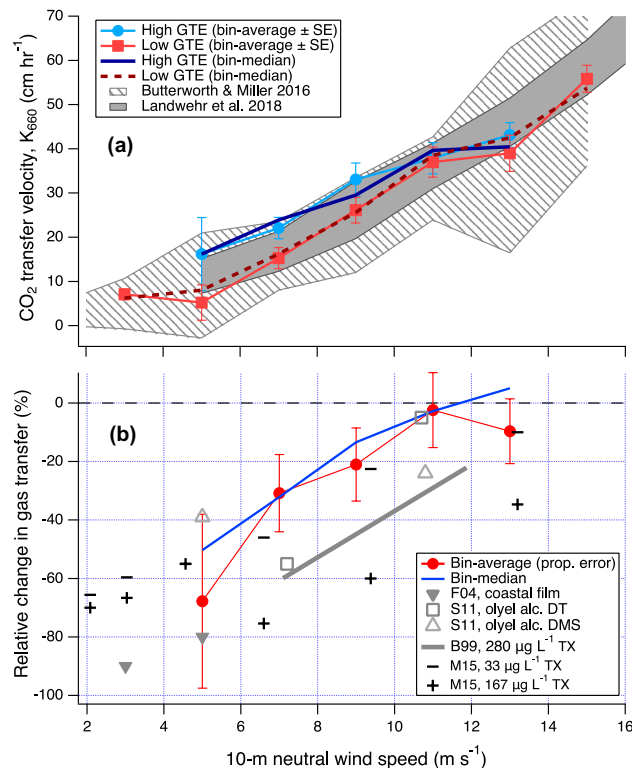


Figure 3. (a) K_{660} vs. 10-m neutral wind speed, separated according to high and low GTE (mean and medium in wind speed bins). K_{660} with high GTE clearly lies above K_{660} with low GTE. To illustrate the variability in previous observations, results from ref.^{10,11} are shown as bin average ± 1 standard deviation (computed from hourly data). (b) Relative change in K_{660} explainable by GTE, which was greatest at low wind speeds and diminished towards high wind speeds during this transect. Also shown are previous estimates of gas transfer suppression due to surfactants based on heat transfer measurements in coastal waters (F04; ref.²⁴), based on two types of gas transfer measurements in patches of an artificial insoluble surfactant (S11; ref.⁴⁸), and based on measurements in laboratory wind-wave tanks with a soluble surfactant (B99 and M15; ref.^{49,50}). For these earlier measurements, relative suppression was computed as ratio in transfer velocity between surfactant-covered and cleaned waters, and U_{10n} was converted from the reported friction velocity where necessary using the COARE 3.5 model.

further, we separate K_{660} measurements into groups of “high GTE” (above 0.582) and “low GTE” (below 0.540). These thresholds correspond to the peaks of the two modes in Fig. 1, and yield about a quarter of all K_{660} measurements in both the high GTE and low GTE groups. The bin-average and bin median of K_{660} associated with high GTE and low GTE are shown in Fig. 3a, with both groups largely residing within the variability of recent K_{660} observations by ref.^{10,11}.

At wind speeds below 11 m s⁻¹, the average K_{660} in the high GTE group is clearly greater than the average K_{660} in the low GTE group. We can estimate the relative effect of varying seawater composition and hydrodynamics on gas transfer from the ratio of low GTE K_{660} to high GTE K_{660} : 100% ($K_{660\text{lowGTE}}/K_{660\text{highGTE}} - 1$). As shown in Fig. 3b, the greatest relative change in K_{660} explainable by GTE was observed at low wind speeds (at least 50% at wind speeds below 5 m s⁻¹) and this change was reduced to ~30% at the global mean wind speed (~7 m s⁻¹). At wind speeds above ~11 m s⁻¹, K_{660} was no longer obviously sensitive to GTE.

How does our measure of relative change in K_{660} explainable by GTE compare against earlier estimates of gas transfer suppression due to the known presence of surfactants? Measurements of natural waters in a tank on a North–South transect through the Atlantic Ocean (45° N to 40° S) suggest up to 32% relative gas transfer suppression due to surfactants¹⁷. Chamber measurements in other marine environments show a 23% relative gas transfer suppression when the SML surfactant concentration exceeds a threshold of 200 $\mu\text{g L}^{-1}$ Triton-X-100 equivalent, and a further 62% suppression in the presence of surfactant films (over 1 mg L⁻¹ Triton-X-100 equivalent)¹⁸. Field observations by Frew et al.²⁴ were made in the presence of coastal surfactant films at very low wind speeds, suggesting significant contributions from insoluble surfactants. Brockmann et al. (ref.⁵¹) and Salter et al. (ref.⁴⁸) released an artificial insoluble surfactant (oleyl alcohol) over km²-sized patches in the North Sea and in the northeast Atlantic Ocean, respectively. The surfactant additions resulted in a ~30% reduction in CO₂ transfer inside of a floating chamber⁵¹ and up to 55% and 39% reductions in the transfer of ³He/SF₆ (dual tracer) and dimethyl sulfide (DMS)⁴⁸. In wind-wave tanks, Bock et al. (ref.⁴⁹) and Mesarchaki et al. (ref.⁵⁰) added a soluble surfactant (Triton-X-100) at bulk concentrations within the range of open ocean surfactant observations^{18,22}; higher concentrations of Triton-X-100 generally resulted in greater gas transfer suppression.

These field and laboratory estimates of gas transfer suppression, regardless of methods employed or surfactants studied, show broadly similar magnitudes as well as similar wind speed dependencies compared to our measurements (Fig. 3b). This implies that the variation in GTE from this transect could also be due to changing natural surfactants. The relative gas transfer suppression decreases with increasing wind speed probably because at least two factors are important in determining the impact of surfactants on near surface hydrodynamics and on gas transfer: molecular composition (e.g. surfactant speciation and concentration) of the near surface water as well as physical turbulence. The GTE measurement captures the range of composition in the subsurface water at a fixed turbulence level within the SFCE system (i.e. independent of wind speed) but this is an inexact representation of the surfactants at the air–sea interface. The persistence of surfactants in the SML depends in part on the mechanism(s) available to transfer them towards/away from the interface. Gas transfer suppression by surfactants is greatest at low wind speeds, when surfactants can accumulate more easily. Wind-driven turbulence and breaking waves seem to be responsible for both the dispersion of the SML and its replenishment via mixing and rising bubbles^{14,52}. In high winds, the degree of suppression is reduced, probably because surfactants at the air–sea interface are dispersed faster than they are replenished.

Theory and laboratory studies (e.g. ref.^{53,54}) suggest that in very low winds or at high surfactant concentrations, the Schmidt number scaling in K_{660} follows an exponent that is closer to $-2/3$ (suitable for a “smooth” surface) than $-1/2$ (suitable for a “rough”, free surface and almost universally applied for the open ocean). For this transect, the difference between $(660/Sc)^{-1/2}$ scaling and $(660/Sc)^{-2/3}$ scaling amounts to about 20%, which is less than our estimate of relative change in K_{660} explainable by GTE at low to moderate wind speeds. This suggests that surfactants may not only change the sea surface characteristics between “smooth” and “rough”, but also alter the amount of turbulence near the sea surface.

Implications for air–sea gas transfer and estimates of global CO₂ flux. The Southern Ocean observations here show that at low-to-moderate wind speeds, the wind speed dependencies in K_{660} can vary by 30% or more, depending on seawater composition. Given the large variability in surfactants both in space^{18,22} and in time²⁵, K_{660} derived from a single area in a single season is unlikely to be representative of the global ocean. Mustaffa et al. (ref.¹⁸) speculated on the global implications of surfactants on air–sea gas exchange, focusing primarily on two aspects: (1) generally lower surfactant concentration and less gas transfer suppression in the open ocean compared to nearshore waters, and (2) the occurrence of surfactant films. Considering the combined effect of wind speed and surfactants on near surface hydrodynamics, how significant are the findings of this study for global/regional air–sea CO₂ flux estimates?

Our data do not necessarily imply that the current global air–sea CO₂ flux should be adjusted downwards in magnitude, but highlight the uncertainty in our understanding. Widely-used parameterizations of K_{660} based on artificially released tracers (e.g. ref.^{47,55}) or the imbalance of radiocarbon (e.g. ref.^{42,56}) incorporated data from many locations/seasons and, to some extent, encompassed a range of biogeochemical and surfactant conditions. Even so, applying these parameterizations to estimate the global or regional CO₂ fluxes may still lead to biases due to surfactants. This is because the spatial variation in surfactant concentration is very large^{18,22} and the biogeochemical controls of surfactants are not well understood. Furthermore, the air–sea CO₂ concentration difference and winds are spatially inhomogeneous and seasonally asynchronous. For example, the tropical oceans tend to have lower wind speeds and are regions of net CO₂ outgassing to the atmosphere, whereas the mid/high latitudes tend to have higher wind speeds and are net sinks of atmospheric CO₂. Stronger relative gas transfer suppression in the tropics due to surfactants (whether linked to lower wind speed—see Fig. 3b, or to higher temperatures—see ref.¹⁷) could impede the outgassing of oceanic CO₂ and potentially lead to a greater net global CO₂ uptake than the current estimate (as postulated also by ref.⁵⁷). We note here that the enhanced suppression of gas transfer in warmer waters suggested by Pereira et al. (ref.¹⁷) was not observed by Mustaffa et al. (ref.¹⁸). The very small temperature range in these Southern Ocean observations (0.7 ± 0.5 °C) precludes any investigation of temperature dependence in the GTE– K_{660} relationship.

The role of biogeochemistry in determining the natural surfactant abundance remains poorly understood. Our measurements of GTE in presumably organic-depleted deep seawater show a mean (standard deviation) value of 0.632 (0.029). GTE in the near surface water is on average 10% lower than in deep water, which is consistent with biological or light driven surfactants sources. However, we did not find any strong relationships between underway GTE and bulk surface biological and physical parameters (see Supplementary Figs. S5–S7), similar to findings by Goldman et al. (ref.²³). Wurl et al. (ref.⁴⁶) found that surfactant concentration tends to be higher in more biologically productive waters. Calleja et al. (ref.⁵⁸) observed reduced CO₂ transfer from a floating chamber over the open ocean in association with higher concentrations of total surface organic matter concentration. Nightingale et al. (ref.⁵⁹) presented contrasting evidence, observing no clear reduction in K_{660} during the development of a large algal bloom in the equatorial Pacific. The gas transfer suppression observed by Pereira et al. (ref.¹⁷) was more pronounced in oligotrophic, rather than biologically productive, waters. No relationship using all cruise data was observed between surfactant concentration and either chlorophyll a concentration (at the time of sampling/2 weeks prior to sampling) or primary production in the Atlantic, possibly because of the influences of bacterial activity²² or photochemical processing⁵². Our work shows that in situ GTE measurements, in combination with direct fluxes by eddy covariance flux observations, provide additional insight into the variance in the gas transfer velocity vs. wind speed dependence. Studies that combine these measurements along with observations of surfactant concentration and other supporting biogeochemical parameters are needed to elucidate the effect of natural organics on gas transfer.

Received: 26 March 2021; Accepted: 18 June 2021

Published online: 30 June 2021

References

1. Khatiwala, S. *et al.* Global ocean storage of anthropogenic carbon. *Biogeosciences* **10**, 2169–2191 (2013).
2. Friedlingstein, P. *et al.* Global carbon budget 2019. *Earth Syst. Sci. Data*. **11**, 1783–1838 (2019).
3. Takahashi, T. *et al.* The changing carbon cycle in the Southern Ocean. *Oceanography* **25**, 26–37 (2012).
4. Frölicher, T. L. *et al.* Dominance of the Southern Ocean in anthropogenic carbon and heat uptake in CMIP5 models. *J. Clim.* **28**, 862–886 (2015).
5. Landschützer, P. *et al.* The reinvigoration of the Southern Ocean carbon sink. *Science* **349**, 1221–1224 (2015).
6. Rhein, M. *et al.* Observations: Ocean. In *Climate Change 2013: The Physical Science Basis. Contribution of Working Group I to the Fifth Assessment Report of the Intergovernmental Panel on Climate Change* (eds Stocker, T. F. *et al.*) (Cambridge University Press, 2013).
7. Woolf, D. K. *et al.* Key uncertainties in the recent air–sea flux of CO₂. *Glob. Biogeochem. Cycl.* **33**, 1548–1563 (2019).
8. Wanninkhof, R., Asher, W. E., Ho, D. T., Sweeney, C. S. & McGillis, W. R. Advances in quantifying air–sea gas exchange and environmental forcing. *Ann. Rev. Mar. Sci.* **1**, 213–244 (2009).
9. Edson, J. B. *et al.* Direct covariance measurement of CO₂ gas transfer velocity during the 2008 Southern ocean gas exchange experiment: Wind speed dependency. *J. Geophys. Res.* **116**, C00F10 (2011).
10. Butterworth, B. J. & Miller, S. D. Air–sea exchange of carbon dioxide in the Southern Ocean and Antarctic marginal ice zone. *Geophys. Res. Lett.* **43**, 7223–7230 (2016).
11. Landwehr, S. *et al.* Using eddy covariance to measure the dependence of air–sea CO₂ exchange rate on friction velocity. *Atm. Chem. Phys.* **18**, 4297–4315 (2018).
12. Blomquist, B. W. *et al.* Wind speed and sea state dependencies of air–sea gas transfer: Results from the high wind speed gas exchange study (HiWinGS). *J. Geophys. Res. Oceans* **122**, 8034–8062 (2017).
13. Brumer, S. E. *et al.* Wave-related Reynolds number parameterizations of CO₂ and DMS transfer velocities. *Geophys. Res. Lett.* **44**, 9865–9875 (2017).
14. Woolf, D. K. Bubbles and their role gas exchange. In *The Sea Surface and Global Change* (eds Liss, P. S. & Duce, R. A.) 173–205 (Springer, 2005).
15. Bell, T. G. *et al.* Estimation of bubble-mediated air–sea gas exchange from concurrent DMS and CO₂ transfer velocities at intermediate–high wind speeds. *Atmos. Chem. Phys.* **17**, 9019–9033 (2017).
16. Frew, N. M., Goldman, J. C., Dennett, M. R. & Johnson, A. S. Impact of phytoplankton-generated surfactants on air–sea gas exchange. *J. Geophys. Res.* **95**, 3337–3352 (1990).
17. Pereira, R. *et al.* Reduced air–sea CO₂ exchange in the Atlantic Ocean due to biological surfactants. *Nat. Geosci.* **11**, 492–496 (2018).
18. Mustafa, N. I. H., Ribas-Ribas, M., Banko-Kubis, H. M. & Wurl, O. Global reduction of in situ CO₂ transfer velocity by natural surfactants in the sea-surface microlayer. *Proc. R. Soc. A* **476**, 20190763 (2020).
19. Liss, P. & Martinelli, F. The effect of oil films on the transfer of oxygen and water vapour across an air–water interface. *Thalass Jugosl.* **14**, 215–220 (1978).
20. Liss, P. Gas transfer: Experiments and geochemical implications. In *Air–sea Exchange of Gases and Particles* (eds Liss, P. & Slinn, W.) 241–298 (Springer, 1983).
21. Garbe, C. S. *et al.* Transfer across the air–sea interface. In *Ocean–Atmosphere Interactions of Gases and Particles* (eds Liss, P. S. & Johnson, M. T.) 55–112 (Springer, 2014).
22. Sabbaghzadeh, B., Upstill-Goddard, R. C., Beale, R., Pereira, R. & Nightingale, P. D. The Atlantic Ocean surface microlayer from 50° N to 50° S is ubiquitously enriched in surfactants at wind speeds up to 13ms⁻¹. *Geophys. Res. Lett.* **44**, 2852–2858 (2017).
23. Goldman, J. C., Dennett, M. R. & Frew, N. M. Surfactant effects on air–sea gas exchange under turbulent conditions. *Deep Sea Res.* **35**, 1953–1970 (1988).
24. Frew, N. M. *et al.* Air–sea gas transfer: Its dependence on wind stress, small-scale roughness, and surface films. *J. Geophys. Res.* **109**, C08S17 (2004).
25. Pereira, R., Schneider-Zapp, K. & Upstill-Goddard, R. C. Surfactant control of gas transfer velocity along an offshore coastal transect: Results from a laboratory gas exchange tank. *Biogeosciences* **13**, 3981–3989 (2016).
26. Miller, S. D., Marandino, C. & Saltzman, E. S. Ship-based measurement of air–sea CO₂ exchange by eddy covariance. *J. Geophys. Res.* **115**, D02304 (2010).
27. Blomquist, B. W. *et al.* Advances in air–sea CO₂ flux measurement by eddy correlation. *Bound.-Lay. Meteorol.* **152**, 245–276 (2014).
28. Landwehr, S., Miller, S. D., Smith, M. J., Saltzman, E. S. & Ward, B. Analysis of the PKT correction for direct CO₂ flux measurements over the ocean. *Atmos. Chem. Phys.* **14**, 3361–3372 (2014).
29. Prytherch, J. *et al.* Motion-correlated flow distortion and wave-induced biases in air–sea flux measurements from ships. *Atmos. Chem. Phys.* **15**, 10619–10629 (2015).
30. Edson, J. B., Hinton, A. A., Prada, K. E., Hare, J. E. & Fairall, C. W. Direct covariance flux estimates from mobile platforms at sea. *J. Atmos. Ocean. Technol.* **15**, 547–562 (1998).
31. Moat, B. & Yelland, M. Airflow distortion at instrument sites on the RRS James Clark Ross during the WAGES project. In *National Oceanography Centre Internal Document 12* (2015).
32. Edson, J. B. *et al.* On the exchange of momentum over the open ocean. *J. Phys. Oceanogr.* **43**, 1589–1610 (2013).
33. Yang, M. *et al.* Comparison of two closed-path cavity-based spectrometers for measuring air–water CO₂ and CH₄ fluxes by eddy covariance. *Atmos. Meas. Tech.* **9**, 5509–5522 (2016).
34. Rella, C. W. *et al.* High accuracy measurements of dry mole fractions of carbon dioxide and methane in humid air. *Atmos. Meas. Tech.* **6**, 837–860 (2013).
35. Foken, T. & Wichura, B. Tools for quality assessment of surface-based flux measurements 1. *Agric. For. Meteorol.* **78**, 83–105 (1996).
36. Vickers, D. & Mahrt, L. Quality control and flux sampling problems for tower and aircraft data. *J. Atmos. Ocean. Technol.* **14**, 512–526 (1997).
37. Dong, Y., Yang, M., Bakker, D. C. E., Kitidis, V. & Bell, T. G. Uncertainties in eddy covariance air–sea CO₂ flux measurements and implications for gas transfer velocity parameterisations. *Atmos. Chem. Phys.* **21**, 8089–8110 (2021).
38. Kitidis, V., Brown, I., Hardman-Mountford, N. & Lefèvre, N. Surface ocean carbon dioxide during the Atlantic Meridional Transect (1995–2013); evidence of ocean acidification. *Prog. Oceanogr.* **158**, 65–75 (2017).
39. Xie, H., Zafriro, O. C., Wang, W. E. I. & Taylor, C. D. A simple automated continuous-flow-equilibration method for measuring carbon monoxide in seawater. *Environ. Sci. Technol.* **35**, 1475–1480 (2001).
40. Wohl, C. *et al.* Segmented flow coil equilibrator coupled to a proton-transfer-reaction mass spectrometer for measurements of a broad range of volatile organic compounds in seawater. *Ocean Sci.* **15**, 925–940 (2019).
41. Dickson, A. G., Sabine, C. L. & Christian, J. R. Guide to best practices for ocean CO₂ measurements. *PICES Spec. Publ.* **3**, 191 (2007).
42. Wanninkhof, R. Relationship between wind speed and gas exchange over the ocean. *Limnol. Oceanogr. Methods* **12**, 351–362 (2014).

43. Carlson, D. J. Dissolved organic materials in surface microlayers: Temporal and spatial variability and relation to sea state. *Limnol. Oceanogr.* **28**, 415–431 (1983).
44. Engel, A. & Galgani, L. The organic sea-surface microlayer in the upwelling region off the coast of Peru and potential implications for air–sea exchange processes. *Biogeosciences* **13**, 989–1007 (2016).
45. Cunliffe, M. *et al.* Comparison and validation of sampling strategies for the molecular microbial ecological analysis of surface microlayers. *Aquat. Microb. Ecol.* **57**, 69–77 (2009).
46. Wurl, O., Wurl, E., Miller, L., Johnson, K. & Vagle, S. Formation and global distribution of sea-surface microlayers. *Biogeosciences* **8**, 121–135 (2011).
47. Ho, D. *et al.* Measurements of air–sea gas exchange at high wind speeds in the Southern Ocean: Implications for global parameterizations. *Geophys. Res. Lett.* **33**, L16611 (2006).
48. Salter, M. E. *et al.* Impact of an artificial surfactant release on air–sea gas fluxes during deep ocean gas exchange experiment II. *J. Geophys. Res. Oceans* **116**, C11016 (2011).
49. Bock, E. J., Hara, T., Frew, N. M. & McGillis, W. R. Relationship between air–sea gas transfer and short wind waves. *J. Geophys. Res.* **104**, 25821–25831 (1999).
50. Mesarchaki, E. *et al.* Measuring air–sea gas-exchange velocities in a large-scale annular wind–wave tank. *Ocean Sci.* **11**, 121–138 (2015).
51. Brockmann, U. H., Hühnerfuss, H., Kattner, G., Broecker, H. C. & Hentzchel, G. Artificial surface films in the sea area near Sylt. *Limnol. Oceanogr.* **27**, 1050–1058 (1982).
52. Mustafa, N. I. H. *et al.* High-resolution observations on enrichment processes in the sea-surface microlayer. *Sci. Rep.* **8**, 13122 (2018).
53. Deacon, E. L. Gas transfer to and across an air–water interface. *Tellus* **29**, 363–374 (1977).
54. Liss, P. & Merlivat, L. Air–sea gas exchange rates: Introduction and synthesis. In *The Role of Air–sea Exchange in Geochemical Cycling* (ed. Buat-Menard, P.) 113–129 (Springer, 1986).
55. Nightingale, P. D. *et al.* In situ evaluation of air–sea gas exchange parameterizations using novel conservative and volatile tracers. *Glob. Biogeochem. Cycl.* **14**, 373–387 (2000).
56. Sweeney, C. *et al.* Constraining global air–sea gas exchange for CO₂ with recent bomb C-14 measurements. *Glob. Biogeochem. Cycl.* **21**, 2015 (2007).
57. Wanninkhof, R. & McGillis, W. R. A cubic relationship between air–sea CO₂ exchange and wind speed. *Geophys. Res. Lett.* **26**, 1889–1892 (1999).
58. Calleja, M. L., Duarte, C. M., Prairie, Y. T., Agustí, S. & Herndl, G. J. Evidence for surface organic matter modulation of air–sea CO₂ gas exchange. *Biogeosciences* **6**, 1105–1114 (2009).
59. Nightingale, P. D., Liss, P. S. & Schlosser, P. Measurements of air–sea gas transfer during an open ocean algal bloom. *Geophys. Res. Lett.* **27**, 2117–2120 (2000).

Acknowledgements

These measurements were made on the ANDREXII cruise on board of the Royal Research Ship *James Clark Ross* (JCR), which was funded by the UK Natural Environment Research Council's ORCHESTRA project (Grant No. NE/N018095/1). The eddy covariance CO₂ flux observations were made possible through a combination of ORCHESTRA and European Space Agency funding (ESA AMT4OceanSatFlux project, Grant No. 4000125730/18/NL/FF/gp). We thank Andrew Meijers (British Antarctic Survey), the chief scientist of the ANDREXII cruise, as well as all the technical, computing, and engineering support on the JCR for accommodating and supporting our air–sea flux measurements. We further thank Philip Nightingale (PML) for insightful discussions about the role of surfactants on gas transfer, Daniel Phillips (PML) for assistance in laboratory characterization of the SFCEs, and John Prytherch (Stockholm University), Robin Pascal (National Oceanography Centre), and Ian Brooks (University of Leeds) for recommendations concerning the flux system installation on the JCR.

Author contributions

M.Y. designed the gas transfer efficiency measurement system with input from T.B. and C.W. M.Y. and T.B. installed the air–sea flux system on the JCR. M.J.Y. advised on the installation of the flux system on the JCR. M.Y. performed data quality control with input from M.J.Y. and T.B. M.Y. carried out the shipboard measurement with support from C.W. T.S. helped with remote monitoring and quality control of the air–sea flux system. I.B. and V.K. installed and maintained the showerhead pCO₂ system. M.Y. wrote the paper with contributions from all authors.

Competing interests

The authors declare no competing interests.

Additional information

Supplementary Information The online version contains supplementary material available at <https://doi.org/10.1038/s41598-021-92947-w>.

Correspondence and requests for materials should be addressed to M.Y.

Reprints and permissions information is available at www.nature.com/reprints.

Publisher's note Springer Nature remains neutral with regard to jurisdictional claims in published maps and institutional affiliations.



Open Access This article is licensed under a Creative Commons Attribution 4.0 International License, which permits use, sharing, adaptation, distribution and reproduction in any medium or format, as long as you give appropriate credit to the original author(s) and the source, provide a link to the Creative Commons licence, and indicate if changes were made. The images or other third party material in this article are included in the article's Creative Commons licence, unless indicated otherwise in a credit line to the material. If material is not included in the article's Creative Commons licence and your intended use is not permitted by statutory regulation or exceeds the permitted use, you will need to obtain permission directly from the copyright holder. To view a copy of this licence, visit <http://creativecommons.org/licenses/by/4.0/>.

© The Author(s) 2021